AIAA JOURNAL
Vol. 43, No. 1, January 2005

Spectrum Evaluation Method for Wrinkled Membranes

Takashi Iwasa*
Institute of Space and Astronautical Science, Kanagawa 229-8510, Japan
Mindy Jacobson†
NASA Goddard Space Flight Center, Greenbelt, Maryland 20771
and
M. C. Natori‡
Institute of Space and Astronautical Science, Kanagawa 229-8510, Japan

A spectrum evaluation method using the two-dimensional fast Fourier transform is proposed for assessing overall behavior of wrinkled membranes. This method was carried out for a square wrinkled membrane. Wrinkling phenomena of the square membrane, held fixed at three corners and subjected to in-plane shear force at the remaining corner, are investigated. The effects of a varied structural scale, which is related to the ratio of membrane area to membrane thickness, and gravity field on the wrinkled membranes are shown using the proposed spectrum evaluation method. Analysis by this method has been verified by comparing the results of the spectrum evaluation method to that of the traditional methods, which uses cross-sectional deformations and deformation modes for assessing the behavior of the membranes including both wrinkled and slack regions.

Introduction

WITH the need to develop increasingly more efficient and lighter mechanical and structural systems for gossamer spacecraft, many researchers have for decades been experimenting with various types of polymer membranes and working to simulate their behavior. Such membranes have been implemented in the designs of parachutes, high-altitude balloons, inflatable structures (i.e., habitation modules, antennas, and synthetic aperture rader (SAR), solar sails, and sunshields.[1–4] One particular area where the use of these membranes can be helpful is for increasing the efficiency of solar cells. Solar-cell efficiency could be increased beyond inherent capacity by optimizing incident radiation intensity. This would be done mechanically by precisely controlling a thin-film reflector or membrane, the surface beneath which is a substrate covered with solar cells. The degree to which solar-cell power output efficiency can be increased by this concept depends upon the ability to predict and assess wrinkling behavior of membranes as a result of predefined or induced loading conditions, hence allowing support to be optimized for designed surface configuration. Likewise, quantified predictions and evaluations of membrane wrinkling behavior can be used to optimize the surface configuration of other membrane structures.

Historically, many researchers have analyzed membrane wrinkling behavior using tension field theory.[5–12] However, because membranes are treated by this theory to be special structures with negligible bending stiffness membrane wrinkling behavior caused by complex bifurcation must be quantified on the basis of a different theory. Tension field theory is, therefore, suitable only for qualitative evaluations of wrinkling phenomena.

For this reason, wrinkling analyses based on imperfect bifurcation including the geometrically nonlinear characteristics of wrinkles are receiving increased attention.[13–19] In an imperfect bifurcation study, wrinkle amplitude and wavelength as well as the orientation angles of wrinkle and wrinkled regions can be clarified. However, the current literature lacks documentation of an accepted evaluation method for easily and quantitatively assessing overall membrane behavior including both wrinkled and slack regions (specifically wavelength and orientation angle). In view of the increasing numbers of gossamer space structures incorporating membranes currently under design, it is important to create an evaluation method for precisely quantifying overall membrane behavior including both wrinkled and slack regions.

This paper documents a spectrum evaluation method using two-dimensional fast Fourier transform (FFT) for assessing the overall behavior of wrinkled membranes. The investigation of a square wrinkled membrane, held fixed at three corners and subjected to in-plane shear at the remaining one corner, is reported herein. For simulating the surface shape of the square wrinkled membrane, a geometrically nonlinear finite element analysis was carried out using mixed interpolation of tensorial components (MITC) shell elements.[19,20] A spectrum analysis of the square wrinkled membrane revealed the effects of a varied structural scale (scale modeling), which was related to the ratio of membrane area to membrane thickness, and gravity field. Analysis by this method has been verified by comparing the results of the spectrum evaluation method to that of the traditional methods, which uses cross-sectional deformations and deformation modes for assessing the behavior of the membranes including both wrinkled and slack regions.

Numerical Analysis

Analytical Model

Figure 1 shows the membrane model treated in this paper. Wrinkling phenomena of a square membrane, held fixed at three corners and subjected to in-plane shear at the remaining corner, were investigated, and Table 1 shows parameters of the square membrane models studied. The size of the square membrane was 0.2×0.2 m. Varied values of membrane thickness (50, 80, 125, 150, 175, 300, 500, and 1000 μm) were considered for studying the effect of structural scale (L/t), scale modeling, on wrinkling behavior. The square membrane was made of polyimid film (Kapton H-Type). Although

Received 20 January 2004; presented as Paper 2004-1742 at the AIAA/ASME/ASCE/AHS/ASC 45th Structures, Structural Dynamics, and Materials Conference, AIAA/ASME/AHS 12th Adaptive Structures Conference, AIAA 6th Non-Deterministic Approaches Forum, and AIAA 5th Gossamer Spacecraft Forum, Palm Springs, CA, 19–22 April 2004; revision received 21 July 2004; accepted for publication 28 July 2004.

*Research Fellow of Japan Aerospace Exploration Agency, Section of Spacecraft Engineering, 3-1-1 Yoshinodai, Sagamihara; taka@taurus.eng.isas.jaxa.jp.

†Aerospace Engineer, Mechanical Systems Analysis and Simulation Branch, Code 542. Member AIAA.

‡Professor, Section of Spacecraft Engineering, Japan Aerospace Exploration Agency, 3-1-1 Yoshinodai, Sagamihara; mcnatori@isas.jaxa.jp. Member AIAA.

Table 1 Membrane parameters

Parameter	Value
Material	Kapton (H-type)
Size, m^2	0.2×0.2
Thickness, μm	50, 80, 125, 150, 175, 300, 500, 1000

Table 2 Mechanical properties of Kapton

Property	Value
Young's modulus E, MPa	2959.6
Poisson's ratio ν	0.34
Density ρ, kg/m^3	1420
Yield point (5% offset), MPa	123.48

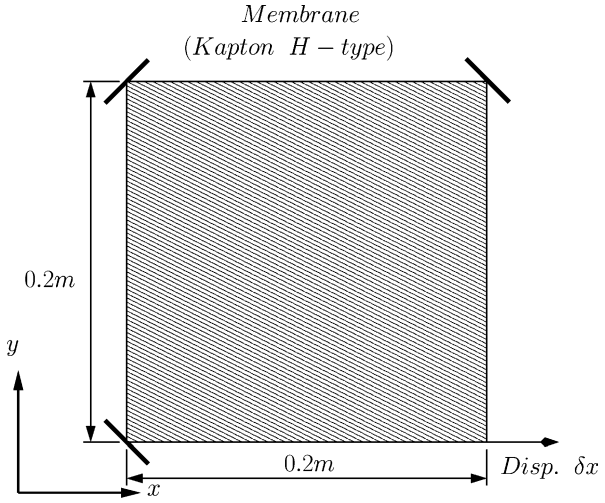

Fig. 1 Membrane model.

Kapton (H-Type) is not readily available in thickness greater than 175 μm, it was nevertheless included in this analytical study in order to thoroughly characterize wrinkling behavior of the illustrated square membrane. Characteristics of the Kapton material were assumed to be linearly elastic, and Table 2 gives a list of the mechanical properties of Kapton H-type made from Du Pont-Toray Co., Ltd.

Finite Element Analysis

A geometrically nonlinear finite element analysis was carried out to simulate wrinkling behavior of the square membrane. The element type used throughout this analysis was a four-node MITC shell element.[20] The number of finite elements used was 10,000. The computational tool used to perform all simulations was the Finite Element Analysis Program: Personal Version (FEAPpv).[21] FEAPpv allows for expansion of the fundamental element library with user-defined functions. The exclusively used four-node MITC shell element employed in this study was added to the FEAPpv library by the authors. In the formation of this element, to improve the accuracy of numerical results, a finite rotation increment of directors was considered in the calculation of the tangent stiffness matrices.[22]

In the case of a geometrically nonlinear analysis using shell elements for wrinkling phenomena, numerical results were intensely affected by mesh aspect ratio, step ratio of numerical analysis, and shape functions of the shell element. Therefore, we investigated these effects on wrinkling analysis focusing on the deformation modes of the wrinkled membranes[15] and confirmed the validity of the numerical results of the finite element (FE) analysis using MITC shell elements.[16–18] The number of finite elements (10,000) used in this study was determined based on an optimization of the aspect ratio for individual elements and for best performance of the four-node MITC shell element, which were given by the previous studies.[15] The effects of the shape function of shell elements, which are those of four- and nine-node MITC shell elements, on wrinkling analysis were inconsequential.[15]

Table 3 Numerical parameters used in the analysis

Parameter	Value
Small displacement δx, mm	1.0
Gravity force G_f	0 or $\rho L^2 tg$
Initial imperfection (NRN), μm	$\pm 0.01\cdot$ membrane thickness

The simulations performed treated imperfect bifurcation phenomena by distributing initial imperfections, node-wise, within the square membrane. The magnitude of initial imperfections was taken from a randomly generated normal-random-number (NRN) distribution, and applied in the out-of-plane direction. Values of initial imperfections were set to be within $\pm 1\%$ of membrane thickness. It was previously confirmed by the authors that the solution convergence and the stress field distribution were significantly affected when the order of magnitude of the initial imperfection was increased over this value.[19]

The in-plane shear force applied at one corner of the square membrane was given as a small displacement δ_x, applied in the x direction, as shown in Fig. 1. The value of the displacement δx was held constant at 1 mm and was determined based on linear elastic behavior of the membrane material. A 1.0-mm displacement was chosen to ensure that no part of the membrane became distorted beyond its capacity to respond elastically.

The gravity force G_f was assumed to act perpendicularly to the plane of the square membrane. For investigating the effects of a gravity field on the wrinkled membrane, this paper simulated wrinkling behavior both with and without the gravity effect. Table 3 lists the parameters used in this study.

Analysis Cases

Table 4 describes and illustrates the analysis cases investigated in this study. Each case was considered for all values of membrane thickness listed in Table 1.

For the "self-weight" case, static effects of a (1-g) gravity field on the square membrane held fixed (five DOF) at all four corners were simulated. Here, the MITC shell element used in this study does not consider the drilling rotation of each node. In the "gravity" case, wrinkling phenomena including the gravity effect were simulated. This case was implemented as the latter part of a two-step geometrically nonlinear solution sequence that commenced with the "self-weight" case already described. The "no gravity–NRN" case does not include the (1-g) gravity effect. Finally, in the "no gravity–sag shape" case the initial condition was provided by the displacements obtained for each thickness simulated in the prior "self-weight" case; the gravity force was removed prior to this set of simulations so that only the displacement field caused by sag was used as the initial condition for this case.

Spectrum Evaluation Method

A spectrum evaluation method using the two-dimensional FFT was considered in order to assess overall behavior of wrinkled membranes. Amplitude, wavelength, and orientation angle of the wrinkled and slack regions within the square membrane were investigated.

The one-dimensional FFT has typically been used to determine the predominant frequency components of complicated wave patterns in the time domain. In the case of the two-dimensional FFT, the orientation angle of waves and their frequency can be quantitatively determined. Figure 2 indicates the sine wave whose spatial frequency in the x and y direction is 10 (1/m), respectively. Therefore, the spatial frequency of this sine wave is 14.14 (1/m) along the direction of 45 deg regarding the x axis. The wavelength of the sine wave is 0.071 m, as it is given by the inverse of the spatial frequency.

The result of the spectrum analysis using two-dimensional FFT for this sine wave is shown in Fig. 3. In this figure, the x and y axis indicate the spatial frequency component, and the z axis indicates the power spectral density. Only the positive domain in the y direction was depicted as a result of the symmetry of the results. From this figure, it is shown that the predominant power spectral density

Table 4 Analysis cases

Cases	Applied load	Initial condition	Boundary condition	Illustration
Self-weight	Gravity force	Imperfection in flatness caused by random distribution of distortion	Five DOF[a] constrained at all four corners	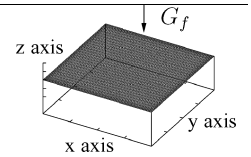
Gravity	Displacement ($\delta x = 1.0$ mm)	Restart of self-weight case	Five DOF[a] constrained at three corners; four DOF constrained at one corner of the applied load	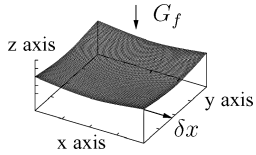
No gravity–NRN	Displacement ($\delta x = 1.0$ mm)	Imperfection in flatness caused by random distribution of distortion	Five DOF[a] constrained at three corners; four DOF constrained at one corner of the applied load	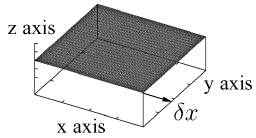
No gravity–sag shape	Displacement ($\delta x = 1.0$ mm)	Sag shape caused by self-weight analysis	Five DOF[a] constrained at three corners; four DOF constrained at one corner of the applied load	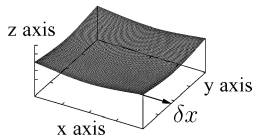

[a]Five-degree-of-freedom (DOF): MITC shell element used does not consider drilling rotation.

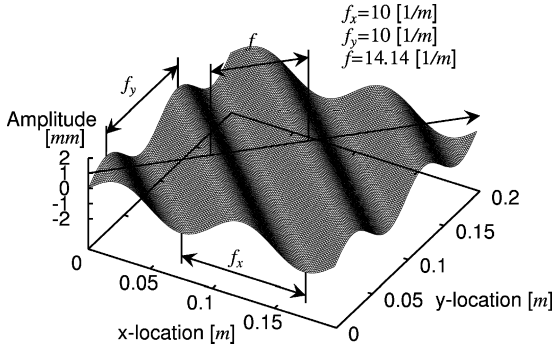

Fig. 2 Sine wave.

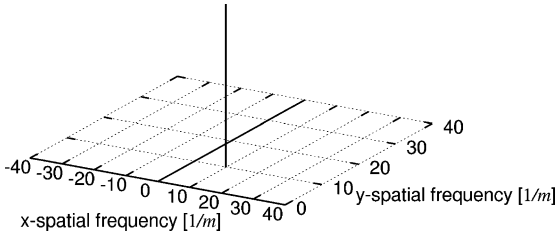

Fig. 3 Result of the spectrum analysis.

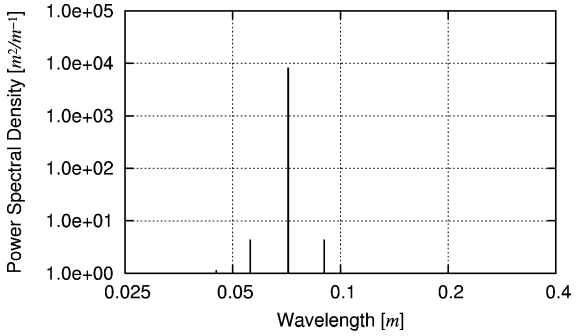

Fig. 4 Wavelength component.

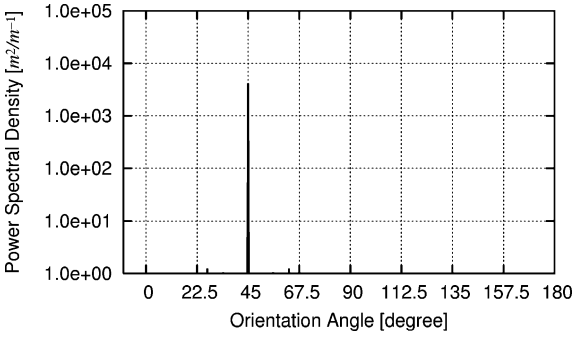

Fig. 5 Orientation angle component.

appeared at (10, 10) in two-dimensional spatial frequency domain. The spatial frequency of the power spectral density in this figure is given by radial distance from the origin, namely,

$$f = \sqrt{f_x^2 + f_y^2} \tag{1}$$

where f_x and f_y coincide with the spatial frequency in the x and y directions. Therefore, $f_{10,10} = 14.14$ [1/m]. Orientation angle θ of the power spectral density is given by

$$\theta = \tan^{-1}(f_y/f_x) \tag{2}$$

The orientation angle of the power spectral density is $\theta_{10,10} = 45$ deg with respect to the x axis. Therefore, this figure reveals both spatial frequency and orientation angle of the sine wave shown in Fig. 2.

Figure 4 indicates the result of the spectrum analysis focusing on the wavelength components. The wavelength is given by the inverse of the spatial frequency. The power spectral density shown in this figure indicates the sum of all power spectral densities located at a constant radial distance in Fig. 3 and were given on a logarithmic scale. In this case, because the spatial frequency of the sine wave is 14.14 [1/m] this figure shows that the wavelength component of the predominant power spectral density is 0.071 m. It is believed that lesser values of power spectral densities correspond to numerical errors appearing in the spectrum analysis because they are three orders (1000 times) lower than the predominant one.

Figure 5 indicates the result of the spectrum analysis focusing on orientation angle components. The power spectral densities shown in this figure indicate the sum of all power spectral densities located at constant orientations in Fig. 3 and were given on a logarithmic scale. Because the orientation angle of the sine wave is 45 deg off

from the x axis, this figure shows that the orientation angle of the predominant power spectral density is 45 deg. It is believed that lesser spectral densities in this figure correspond to those numerical errors on the wavelength components (refer to Fig. 4), as already described.

The power-spectral-density levels given by the spectrum analysis using two-dimensional FFT include two components indicating the prominence of discrete wavelength and orientation angles. These levels reveal relationships between 1) amplitude and wavelength and 2) amplitude and orientation angles because the power spectral density given by the spectrum analysis is related to the amplitude of the wave. Therefore, when the spectrum analysis is employed to evaluate the state of a membrane surface, it is believed that the wavelength (or spatial frequency) and orientation angle of the wave that predominates for the surface feature of the wrinkled membranes can be easily obtained. This is in contrast to conventional studies,[13,14] which used an arbitrary cross-sectional deformation mode or the "bird's-eye" view of the wrinkled membrane for the evaluation and characterization of wrinkling phenomena. In the conventional studies, it is difficult to assess both wavelength and orientation angle of the predominant wave constituting the surface feature of the wrinkled membrane, both easily and quantitatively. The spectrum evaluation method discussed herein offers a new method for clarifying the wavelength and orientation angle components of waves that predominate surface features of wrinkled membranes. Here, the orientation angle given by spectrum analysis using two-dimensional FFT indicates the direction of the wave propagation. Therefore, orientation angles of wrinkles resulting from this method are about 90 deg out of alignment from conventional orientations given by the direction of major principle stresses.

The spectrum evaluation method for assessing wrinkling behavior must be applied with care because the accuracy of the method is sensitive to the sampling number, which in this analysis corresponded to discretization along each axis. For the two-dimensional FFT, the total sampling number along each axis is assumed to be 2^{α} (α: integer). Therefore, there was a discrepancy between the sampling number (2^{α}) and the true resolution of the analytical model, which was given by the number of nodes along any edge of the mesh (101 for the models shown Fig. 1). The sampling points associated with this discrepancy were set to zero in the spectrum analysis. As a result, this discrepancy affected the accuracy of the spectrum evaluation method because it altered slightly the surface feature of the membrane in the spectrum analysis.

Figure 6 indicates the result of the spectrum analysis for the sine wave shown in Fig. 2. In this spectrum analysis, the number of nodes along each axis of the sine wave was set to 101. Therefore, the total sampling number (2^{α}) used in the spectrum analysis was 128 ($\alpha = 7$). Given this value, sampling points in the range of 102 to 128 were set to zero. The ratio of the number of zeros (27) to the total sampling number (128) gave 21% discrepancy. Compared with the result shown in Fig. 3, which was given by the spectrum analysis whose number of nodes along each axis was set to 128, the predominant power spectral density in Fig. 6 was unclear. This effect also appeared in the results focusing on the wavelength and orientation angle shown in Figs. 7 and 8. Therefore, the sampling number should be chosen to be as close to the analytical resolution as possible.

The simplest method for eliminating this discrepancy is to choose a nodal density that corresponds to the sampling number (2^{α}) used in the spectrum analysis. However, in actual situations it is often difficult to determine the specific mesh density because of some analytical or experimental constraints, which are related to the selection of the suitable mesh aspect ratio, computational cost in FE

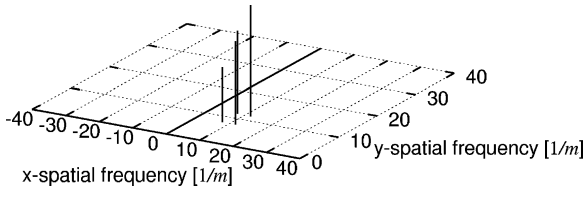

Fig. 6 Result of the spectrum analysis.

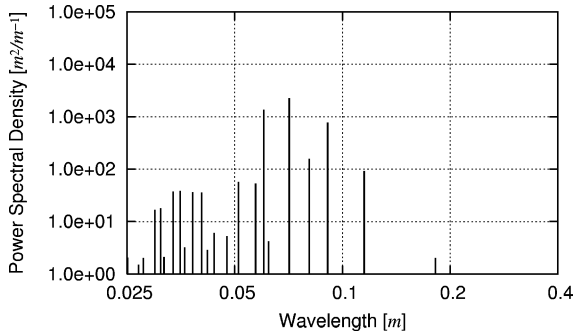

Fig. 7 Wavelength components.

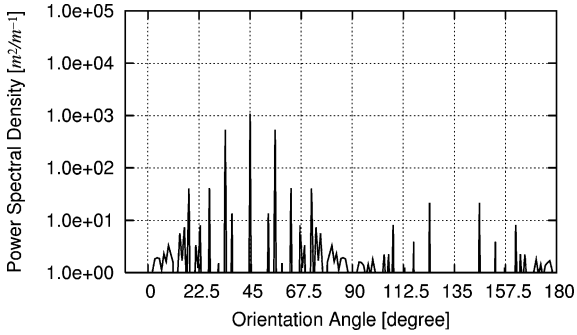

Fig. 8 Orientation angle components.

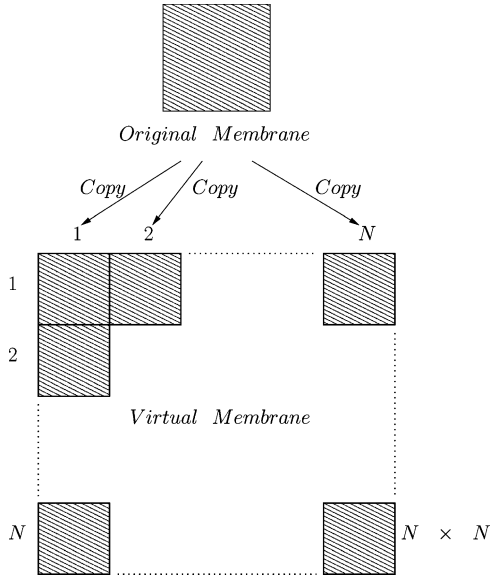

Fig. 9 Virtual membrane.

analysis, measurement method, and cost in experiment. In this paper, an arbitrary sampling number (101) was given in order to show how the solution is affected in the general case where mesh density differs from 2^{α}.

A method employed to both reduce the discrepancy and increase the resolution of the FFT was to create a virtual membrane surface. This virtual membrane, shown in Fig. 9, was constituted by creating a sequence of repeated membranes, each identical to the original. When the number of nodes along any edge of the original membrane is equal to 2^{α}, the virtual membrane corresponds to a part of an infinitely repeated membrane. In the spectrum analysis for the virtual membrane, discontinuities appear at the boundaries of repeated membranes, and effect the accuracy of the spectrum analysis just as the spectrum analysis for the original membrane. A general method that can be employed to reduce the effects of discontinuities in the spectrum analysis is to use a window function such as a Hanning window. However, the spectrum analysis performed in this study did not use any window function because the virtual membrane

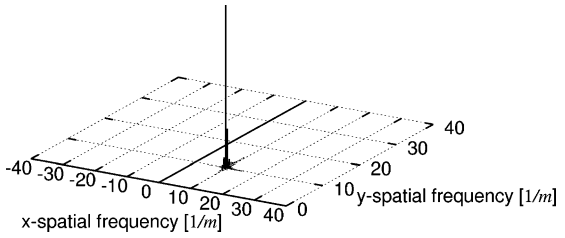

Fig. 10 Result of the spectrum analysis.

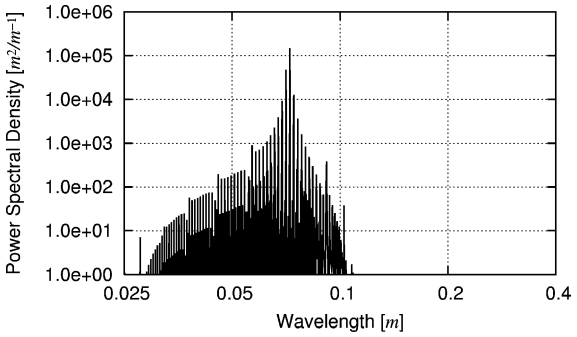

Fig. 11 Wavelength components.

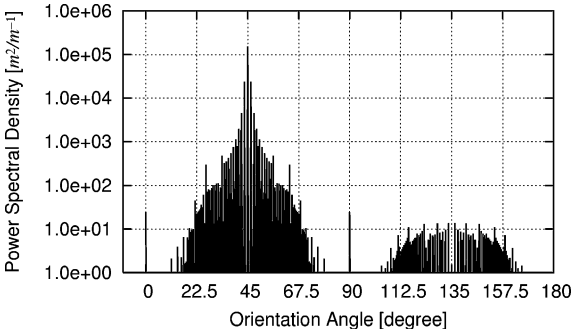

Fig. 12 Orientation angle components.

including discontinuities was constructed before conducting the spectrum analysis. Therefore, all results given by the spectrum analysis in this paper include the effects of the discontinuities, although the effects of the discrepancy related to the sampling number just stated were improved.

The number of repeated membranes N used in the virtual membrane allows the total sampling number (2^{α}) used in the spectrum analysis to be increased. Careful choice of N enables a closer match between number of total FE mesh points and 2^{α}. However, computational cost of the spectrum analysis limits the maximum value of N that is of practical use. In this work, the number of repeated membranes was set to $N = 10$, leading to a virtual membrane containing 1010 nodes per side. For the integral value of α, the next largest sampling number 2^{α} used in the spectrum analysis was $2^{10} = 1024$. In this case, the ratio of the number of zeros (14) to the total sampling number (1024) gave just 1.4% discrepancy. Figures 10–12 indicate the results of the spectrum analysis for the virtual membrane ($N = 10$) and the sine wave introduced earlier. Compared with Figs. 6–8, Figs. 10–12 show that the predominant power spectral densities were clearer, and accuracy of the spectrum evaluation method was improved by introducing the virtual membrane.

Another advantage of using the virtual membrane method is that higher N enables improved spatial frequency resolution. The fundamental spatial frequency f_c of the spectrum analysis using the virtual membrane is

$$f_c = 1/(NL) \tag{3}$$

whereas that using only the original membrane ($N = 1$) is

$$f_c = 1/L \tag{4}$$

This shows how the spatial frequency increment in the spectrum analysis becomes smaller when the virtual membrane is used and N is increased. Therefore, using the virtual membrane in the spectrum analysis permitted more detailed evaluation of the wavelength components (inverse of the spatial frequency) for the wrinkled membrane.

However, when the membrane size is large it is difficult to perform the spectrum evaluation method using the virtual membrane for assessing membrane surface feature. This is because the virtual membrane increases the computational cost of the spectrum analysis as stated before. In this work, introducing the virtual membrane was used as the method for improving effects of the discrepancy related to sampling number in the spectrum analysis. Other suitable nonvirtual membrane methods for the spectrum analysis are considered for future works.

Results and Discussion

Spectrum Analysis

Overall behavior of the square wrinkled membrane is discussed in the context of results obtained from spectrum analyses presented in the preceding section. All figures listed in this subsection represent simulation results for a membrane with thickness equal to 50 μm ($L/t = 4000$) based on the gravity case.

Figure 13 shows a bird's-eye view of the initial state of the simulations, which corresponds to a membrane deformed under its own weight (self-weight case). The result of the spectrum analysis performed using two-dimensional FFT for this deformed membrane is shown in Fig. 14. The power spectral density corresponded to $N = 10$ (a 10×10 virtual membrane) and was shown on a linear scale protruding from the spatial frequency domain. This figure shows that the predominant power spectral densities appeared at (4.88, 0) and (0, 4.88) in the spatial frequency domain. Because the inverse of the edge length of the square membrane is 5.00 [1/m], it is believed that these two spatial frequencies appeared caused by the sequentially repeated deformed membranes. The difference between 4.88 [1/m] and 5.0 [1/m] was related to the discrepancy of the sampling number (1.4%) in the spectrum analysis. Figures 15 and 16 indicate the power spectral densities focusing on the wavelength and orientation angle components, respectively. From these figures, the predominant power spectral densities appeared at 0.205 m for the wavelength component and at 0 and 90 deg for the orientation angle component. These values corresponded to the predominant power spectral densities shown in Fig. 14. Because the sagging geometry of the deformed membrane shown in Fig. 13 was symmetric, the results of the two-dimensional FFT focusing on the orientation angle (refer to Fig. 16) is also symmetric.

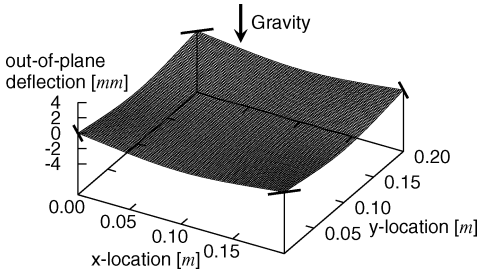

Fig. 13 Deformed membrane ($L/t = 4000$).

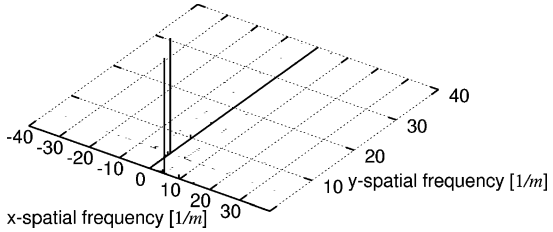

Fig. 14 Result of the spectrum analysis ($L/t = 4000$).

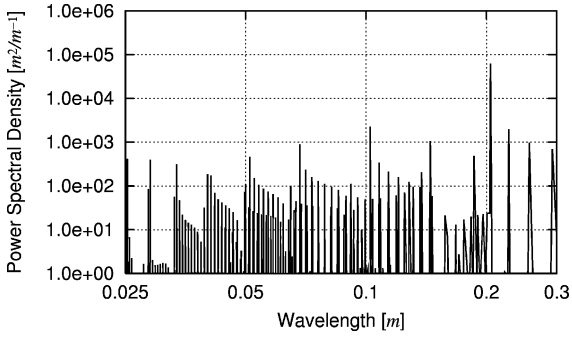

Fig. 15 Wavelength component ($L/t = 4000$).

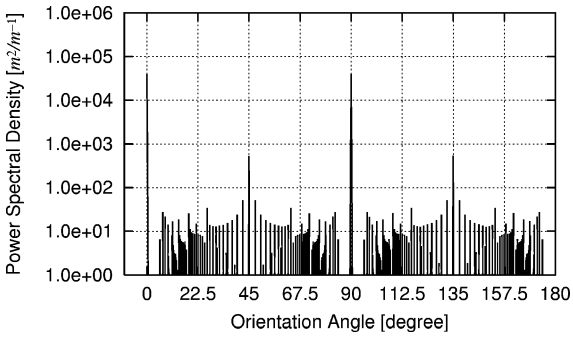

Fig. 16 Orientation angle component ($L/t = 4000$).

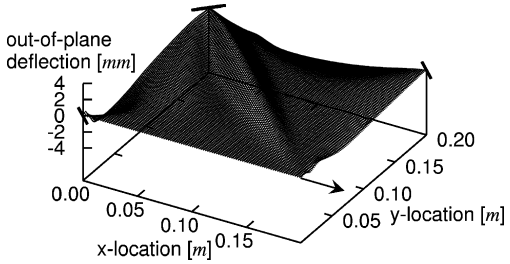

Fig. 17 Wrinkled membrane ($L/t = 4000$).

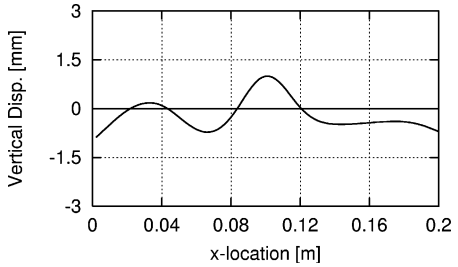

Fig. 18 Membrane midsection ($y = 0.10$ m, $L/t = 4000$).

Figure 17 shows a bird's-eye view of the wrinkled membrane obtained from a FE solution. From this figure, it is clear that major wrinkling was predicted in the −45-deg direction (with respect to the x axis). In addition, two slack regions were predicted to form on both sides of the major wrinkle. This figure shows that the wrinkled region appears to have a short wavelength, whereas the slack regions have long wavelengths. The cross-sectional deformation of the wrinkled membrane ($y = 0.10$ m) is shown in Fig. 18. From this figure, the wavelength of the major wrinkle in the x direction was 0.078 m (from $x = 0.044$ to 0.122 m). Therefore, it is considered that the wavelength in the direction of 45 deg with regards to x axis was 0.055 m, and it corresponded to the maximum wavelength of the major wrinkle (refer to Fig. 17).

The result of a spectrum analysis performed using two-dimensional FFT for this wrinkled membrane is shown in Fig. 19. The maximum frequency treated in these analyses was set to 40. This corresponds to realistic values for minimal wavelength (or

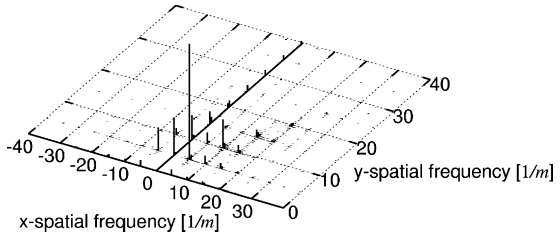

Fig. 19 Result of the spectrum analysis ($L/t = 4000$).

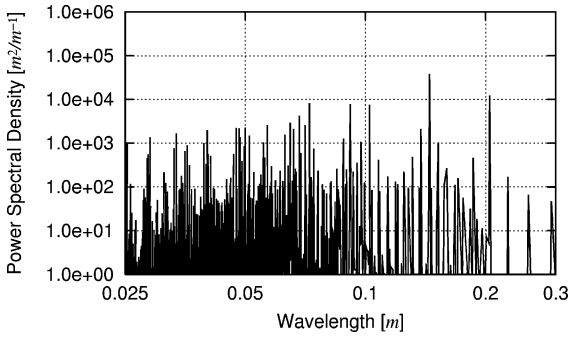

Fig. 20 Wavelength component ($L/t = 4000$).

maximum spatial frequency) components in the wrinkled and slack regions of physical membranes. Figure 19 shows both the spatial frequency and orientation angle of the wrinkled and slack regions in the membrane. The remarkable power spectral densities appearing in this figure were located at the spatial frequency, 4.88 [1/m], interval in both the x and y directions. This interval was determined by the edge length L of the membrane as stated before. Therefore, it turned out that a virtual membrane surface feature was approximated by the waves whose spatial frequency was based on 4.88 [1/m]. The maximum power spectral density was located at (4.88, 4.88) in the spatial frequency domain; this value corresponds to the most prominent virtual membrane surface feature. From this figure, the spatial frequency of the predominant power spectral density was $f_{4.88,4.88} = 6.901$ [1/m]. Because the wavelength is given by the inverse of the spatial frequency, the wavelength of the predominant power spectral density was $\lambda = 0.145$ m. The orientation angle was $\theta_{4.88,4.88} = 45$ deg with respect to the x axis, which can correspond to the major wrinkle feature visible in Fig. 17. In the virtual membrane, the major wrinkle was repeated at the spatial frequency of 6.901 [1/m] ($\lambda = 0.145$ m) interval along the direction of 45 deg regarding to the x axis.

Figure 20 shows the result of the spectrum analysis focusing on the wavelength component. As power spectral density is proportional to the displacement amplitude on the membrane surface, this figure shows that the wavelength components that predominated for the virtual membrane were $\lambda = 0.145$ and 0.205 m. These power spectral densities include the effects of both wrinkled and slack regions, when the wave constituting these region have the same wavelength components. However, it is believed that the power spectral density appearing at $\lambda = 0.145$ m was dominated by the effect of the major wrinkling as just stated, in addition to the other slack regions that were caused by the initial sagging geometry (refer to Fig. 15). In this figure, the power spectral density at the major wrinkling wavelength (0.055 m), which was shown in Fig. 19, did not appear prominently. This is because the amplitude of waves having the wavelength component (0.055 m) was less than that having other wavelength component, when overall virtual membrane surface features were evaluated. For example, a maximum amplitude of the wrinkled membrane appeared in the slack regions, not at the major wrinkle. The significance of this figure is to clarify the wavelength component of waves that were prominent for the complicated surface feature of our virtual wrinkled membrane.

Figure 21 shows the result of the spectrum analysis focusing on the orientation angle. This figure shows that the predominant orientation angles for wrinkled and slack regions were calculated (by FE

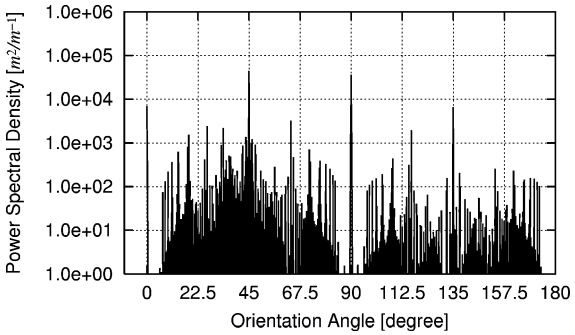

Fig. 21 Orientation angle component ($L/t = 4000$).

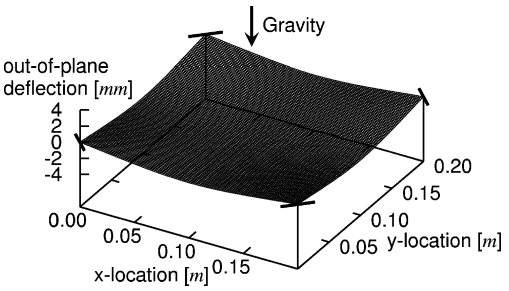

Fig. 22 Deformed membrane ($L/t = 2500$, self-weight case).

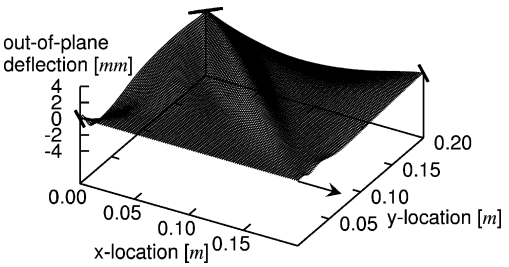

Fig. 23 Wrinkled membrane ($L/t = 2500$, gravity case).

analysis) to be 0, 45, 90, and 135 deg. It is believed that the peak spectrum analysis values obtained at 0 and 90 deg were caused by the initial sagging geometry (refer to Fig. 16). The elevated power spectral densities concentrated in the vicinity of 45 and 135 deg were attributed to the formation of the major wrinkle, induced by the 1-mm corner displacement simulated in the FE analysis. These results for the wavelength and orientation angle also showed that the behavior of the slack regions was as large as that of the wrinkled regions. This means that the studying on the behavior of the slack regions as well as that of the wrinkled regions is significant for gossamer spacecraft whose performance depends on membrane surface features.

In summary, this section verified applicability of the spectrum evaluation method using two-dimensional FFT for assessing overall membrane behavior including both wrinkled and slack regions.

Effects of Structural Scale (Scale Modeling) on Wrinkled Membrane

In this section, the effect of thickness vs wrinkling behavior is discussed using FE results from both the self-weight and gravity cases. Figure 22 shows the bird's-eye view of a membrane ($L/t = 2500$) deformed under its own weight (self-weight case), and Fig. 23 shows a wrinkled membrane ($L/t = 2500$) from the same orientation, obtained by adding a 1-mm corner displacement to the preceding case (gravity case).

Figure 24 compares the results of both cases with respect to maximum displacement ratio. Here, maximum displacement ratio along the ordinate axis is indicated by the ratio of maximum absolute value of displacements amplitude $w_{\max}$ to membrane thickness t. Structural scale given along the abscissa is a nondimensionalized

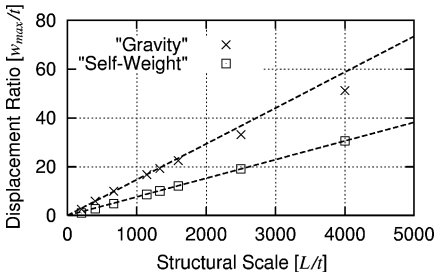

Fig. 24 Maximum displacement ratio.

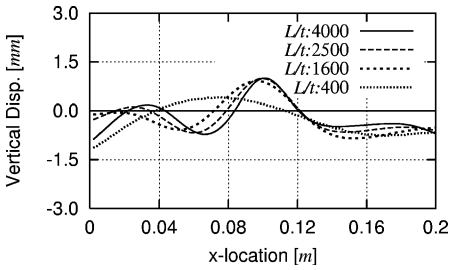

Fig. 25 Membrane midsection ($y = 0.10$ m).

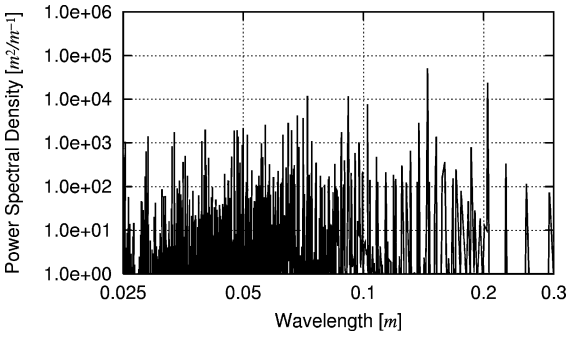

Fig. 26 Wavelength component ($L/t = 2500$).

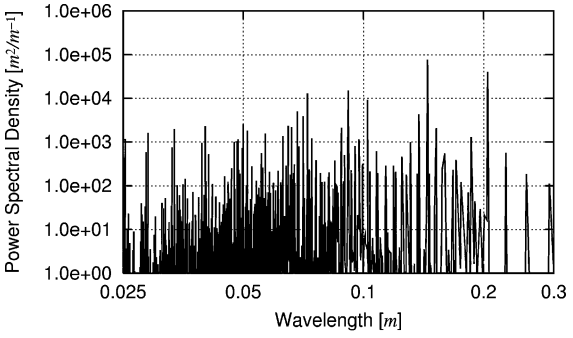

Fig. 27 Wavelength component ($L/t = 1600$).

ratio of edge length L to membrane thickness t. This figure shows that displacement ratio increased linearly with structural scale for the self-weight case, whereas displacement ratio vs structural scale for the gravity case became slightly nonlinear for abscissa values that exceed 1500. This nonlinear phenomenon is related to the relationship between membrane thickness and bending stiffness and has been studied from the viewpoint of strain energy by the authors.[18]

Figure 25 shows deformation modes along the midsection, $y = 0.10$ m, of the square wrinkled membrane. From this figure, it is clear that wavelength increased and amplitude decreased, as the membrane structural scale was decreased. However, overall wrinkling behavior of membranes caused by the gravity cases cannot be fully characterized using midsection analysis as only local behavior is indicated. As a result, the just discussed spectrum evaluation method for investigating overall behavior was again carried out. Figures 26–28 show the power spectral densities focusing on the

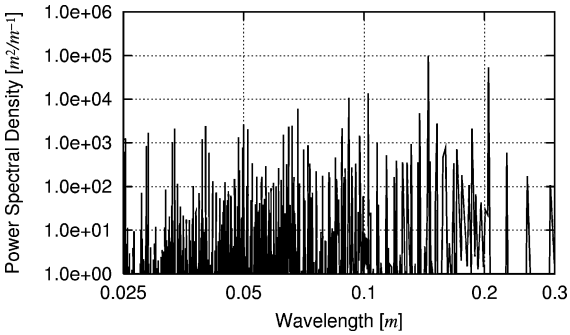

Fig. 28 Wavelength component ($L/t = 400$).

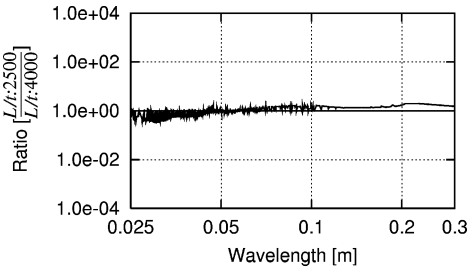

Fig. 29 Wavelength component ($L/t = 2500, 4000$).

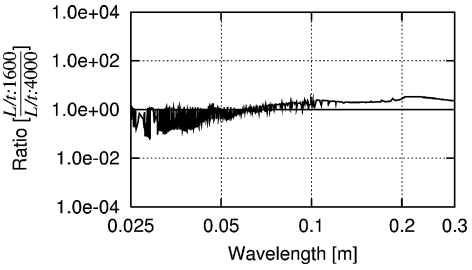

Fig. 30 Wavelength component ($L/t = 1600, 4000$).

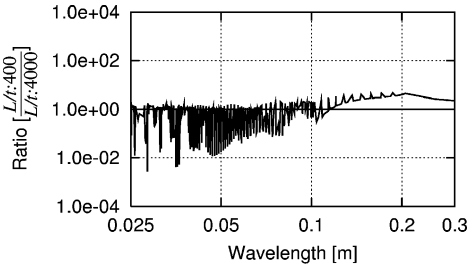

Fig. 31 Wavelength component ($L/t = 400, 4000$).

wavelength components. Comparative results of the power spectral densities for smaller structural scale values (2500, 1600, and 400) relative to the maximum structural scale of 4000 are shown Figs. 29–31 to understand clearly effects of the structural scale on overall membrane behavior. In general, it can be seen from these figures that as structural scale decreased power spectral densities of the longer wavelength components increased, while those corresponding to shorter wavelength components were decreased. Additionally, Figs. 29–31 show that the regions dominated by short-wavelength components were extended as structural scale was decreased. These results correspond to the physical wrinkling characteristics, in which long-wavelength components are dominant in surface features of a wrinkled membrane having low structural scale L/t (refer to Fig. 25). Therefore, these results can also be used to describe local behavior of deformation modes in Fig. 25.

Figures 32–34 show the power spectrum densities focusing on the orientation angle components, and Figs. 35–37 show comparative

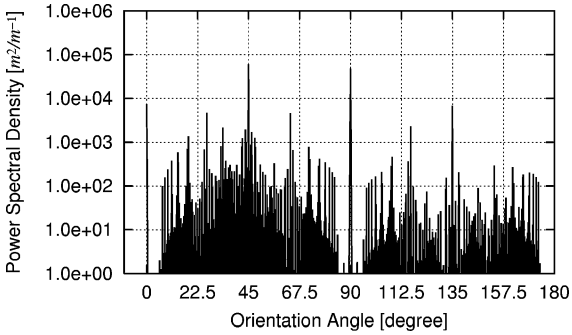

Fig. 32 Orientation angle component ($L/t = 2500$).

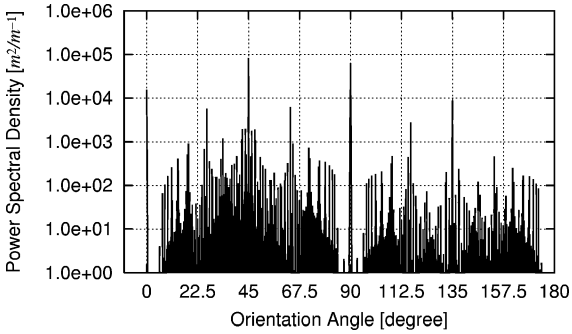

Fig. 33 Orientation angle component ($L/t = 1600$).

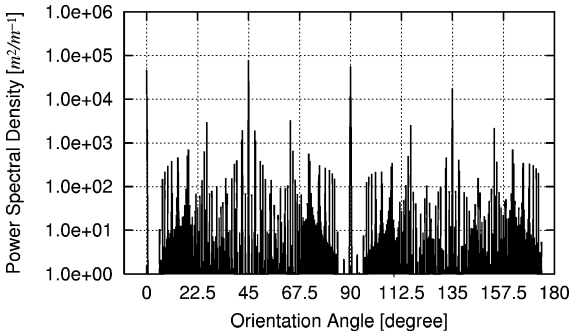

Fig. 34 Orientation angle component ($L/t = 400$).

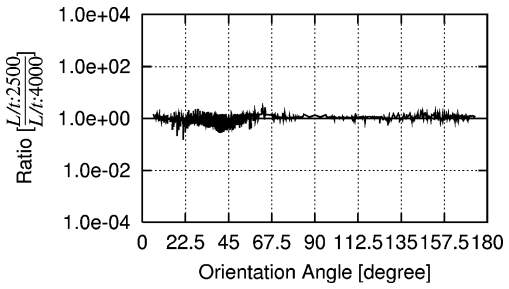

Fig. 35 Orientation angle components ($L/t = 2500, 4000$).

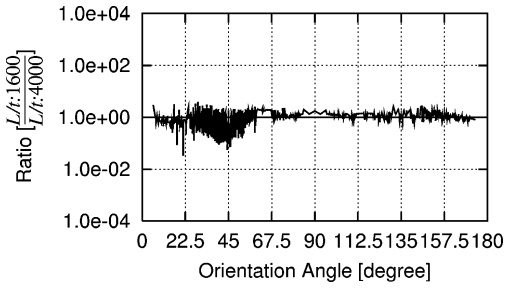

Fig. 36 Orientation angle components ($L/t = 1600, 4000$).

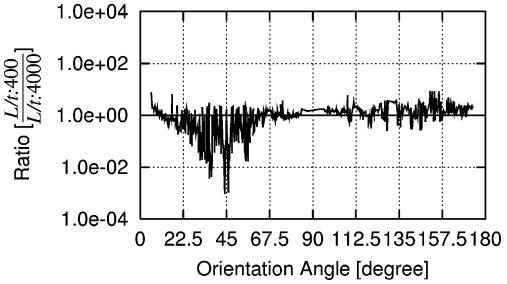

Fig. 37 Orientation angle components ($L/t = 400$, 4000).

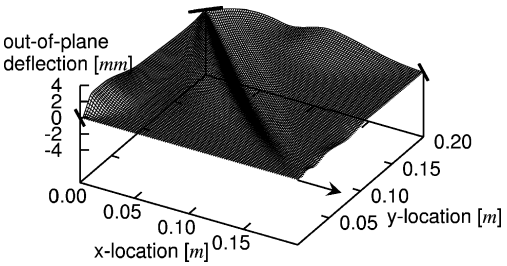

Fig. 38 Wrinkled membrane ($L/t = 4000$, no gravity–NRN).

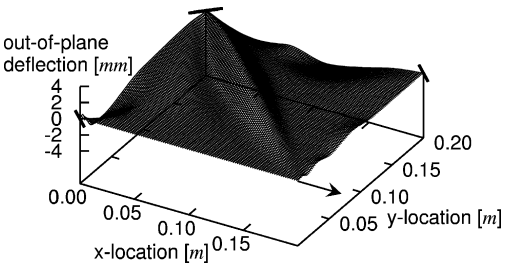

Fig. 39 Wrinkled membrane ($L/t = 4000$, no gravity–sag shape).

results of the power spectral densities for smaller structural scale values (2500, 1600, and 400) relative to the maximum structural scale of 4000. These figures indicated that, when structural scale became small, power spectral densities corresponding to orientation components in the range of 0–60 deg decreased dramatically. The most predominantly affected regions fell within the range of 30–60 deg. However, in the range of 60–180 deg, power spectral density only slightly increased, with no clear domination in any particular range of angular orientations.

When considering both wavelength and orientation angle components together, across the entire membrane surface the results showed that power spectral densities with orientation components in the range of 0–60 deg consisted predominantly of short-wavelength components (as is shown in Figs. 29–31). Similarly, power spectral densities with orientations in the range of 60–180 deg consisted predominantly of long-wavelength components. Assuming that short-wavelength components correspond to wrinkled regions and long-wavelength components correspond to slack regions, these results indicate that the behavior of wrinkled regions is highly dependent on structural scale. Because the wrinkling phenomena are kinds of the bifurcation events, these results indicate that the wrinkling characteristics are highly dependent on the membrane thickness.

In summary, this section indicated that the effects of structural scale on overall behavior of wrinkled membranes can be assessed by using the spectrum evaluation method.

Effects of Gravity Force

In this section, the gravity field effects on wrinkling behavior were investigated by comparing the results of the gravity, no gravity–NRN, and no gravity–sag shape FE simulations using the spectrum evaluation method. Figures 38 and 39 show bird's-eye views of the wrinkled membranes computed using no gravity–NRN and no gravity–sag shape initial conditions, respectively. In the no gravity–NRN case, the computed deformed shape depended on the shape of the initial imperfection, and Fig. 38 shows one example of the shapes deformed in the reverse direction with respect to the z axis. Figure 39 shows an example of the deformed membrane contour computed using the no gravity–sag shape initial conditions. The distortion shown here is greater than that obtained using similar initial condition (refer to Fig. 17).

Figure 40 shows the result with respect to a maximum displacement (or, amplitude) ratio $w_{\max}/t$. It is clear from this figure that when structural scale was greater than 1500 gravity force effects appeared gradually and were more significant for the gravity case than for the no gravity–NRN case. Data points in this figure simply corresponded to slack regions, although each point appeared in different locations of the slack regions. Therefore, from this figure it turns out that gravity field effects on slack regions appear intensely with increasing structural scale.

The comparative results from the gravity and no gravity–NRN cases with respect to wavelength components at structural scales of 200, 1333, and 4000 were presented in Figs. 41–43. Results

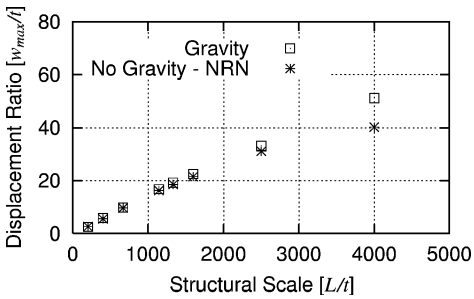

Fig. 40 Maximum displacement ratio.

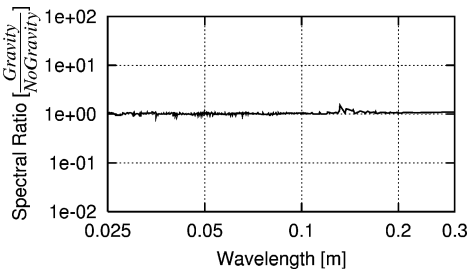

Fig. 41 Wavelength components ($L/t = 200$).

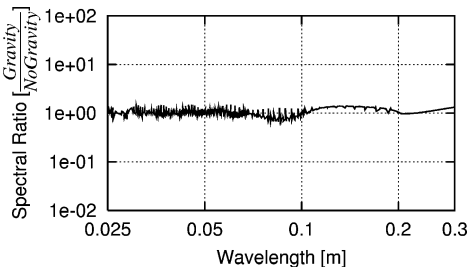

Fig. 42 Wavelength components ($L/t = 1333$).

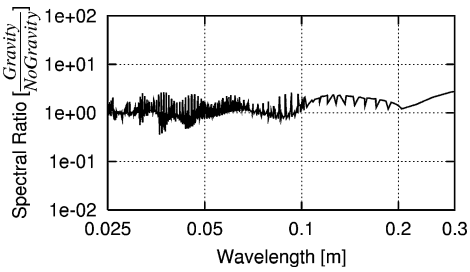

Fig. 43 Wavelength components ($L/t = 4000$).

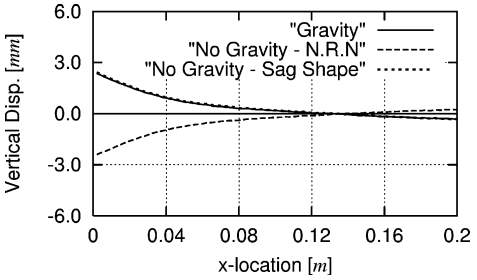

Fig. 44 Cross-sectional deformation ($y = 0.04$ m, $L/t = 200$).

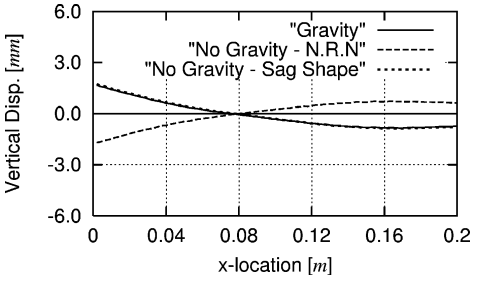

Fig. 45 Cross-sectional deformation ($y = 0.10$ m, $L/t = 200$).

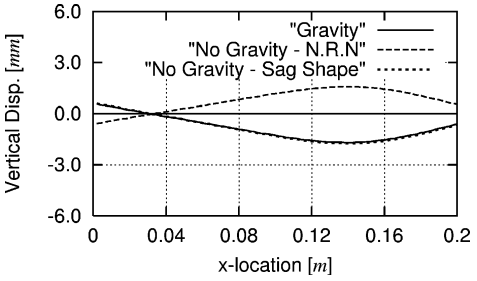

Fig. 46 Cross-sectional deformation ($y = 0.16$ m, $L/t = 200$).

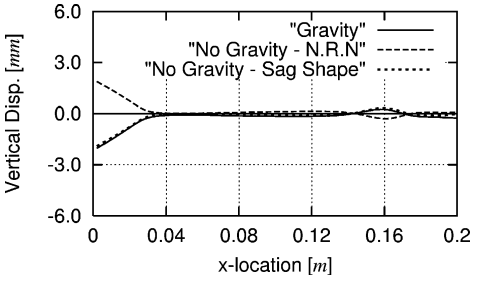

Fig. 47 Cross-sectional deformation ($y = 0.04$ m, $L/t = 4000$).

from Fig. 43 indicate that power-spectral-density levels of long-wavelength components for the gravity case were greater than for the no gravity–NRN case with large structural scale. In contrast, Figs. 40 and 41 show that effects of the gravity field on overall membrane behavior did not appear for low structural scale.

To clarify these results, cross-sectional deformations of wrinkled membranes calculated from the FE analysis were investigated. Figures 44–49 show comparative results with respect to deformation modes given by the gravity, no gravity–NRN, and no gravity–sag shape cases. These were deformation modes along the cross sections, $y = 0.04$, 0.10, and 0.16 m, of each wrinkled membrane for structural scales of 200 and 4000. Figures 44–46 show that for a structural scale of 200, the gravity and no gravity–NRN deformation modes were symmetric. When the deformation modes are symmetric, the same solutions are given by a spectrum analysis. Therefore, it seems reasonable that for small values of structural scale, the deformation modes given by gravity and no gravity–NRN cases should be nearly equivalent as shown in Fig. 41. However,

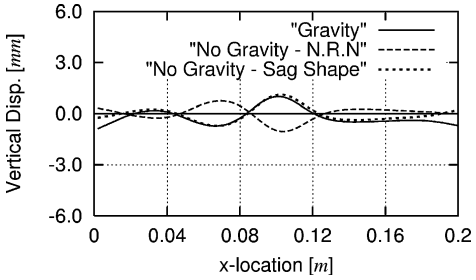

Fig. 48 Cross-sectional deformation ($y = 0.10$ m, $L/t = 4000$).

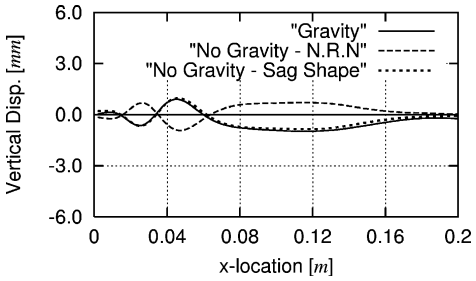

Fig. 49 Cross-sectional deformation ($y = 0.16$ m, $L/t = 4000$).

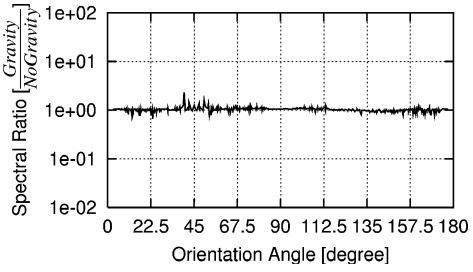

Fig. 50 Orientation angle component ($L/t = 200$).

the results given in Figs. 47–49 clearly indicated that deformation modes, especially in slack regions, were no longer symmetric for a structural scale of 4000. It is believed that this difference was reflected within the results of the spectrum analyses presented in Fig. 43.

Figures 44–49 also present deformation modes from the no gravity–sag shape case. Clearly, the deformation modes from this case were almost identical to those from the gravity case. Therefore, it is believed that gravity field effects on the deformation modes are caused by the initial deformation state of the membrane and are not caused by the effects of an initial stress field caused by the applied gravity force. This means that the effects of an initial stress field on final membrane stresses in the vicinity of bifurcation points, as a result of the (1-g) gravity effect, are practically negligible.

In addition, as can be seen from Figs. 47–49, deformation modes from the three cases were either in agreement or symmetric within wrinkled regions, but were not in agreement within slack regions. As a result, it is considered that effects of the gravity field on wrinkled membranes are most significant in slack regions and increase with increasing structural scale. This consideration can also be used to justify maximum displacement ratio $w_{\max}/t$, as a function of structural scale L/t shown in Fig. 40. Because rigid motion occurs in the slack regions, it is believed that the slack regions are easily effected by the applied forces such a gravity.

These considerations indicate that effects of the gravity field on the wrinkled regions are small. As stated before, wrinkling behavior is intensely affected by the membrane thickness, not a gravity. Therefore, it is believed that ground experiments carried out on prototype space structure hardware would accurately predict the behavior of wrinkled (but not slack) region in space for geometry similar to that of the virtual membrane presented herein.

Figures 50–52 compare results from the gravity and no gravity–NRN cases with respect to orientation angles of each wrinkled

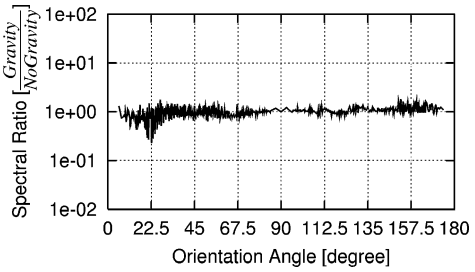

Fig. 51 Orientation angle component ($L/t = 1333$).

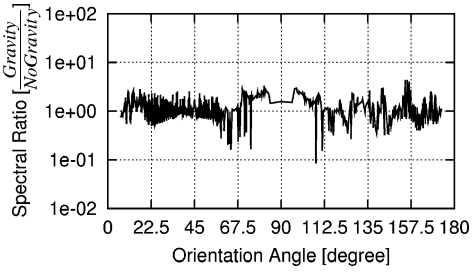

Fig. 52 Orientation angle component ($L/t = 4000$).

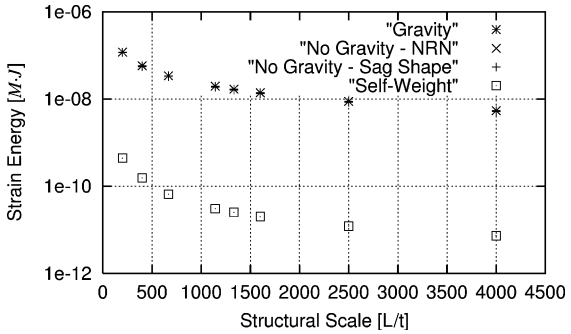

Fig. 53 Strain energy.

membrane. From these figures, it is clear that the gravity field also affected orientation angles as structural scale was increased. However, these deformation effects were not concentrated in any particular regions of the membrane. This tendency was different from the effects of structural scale on wrinkled membranes shown earlier in Figs. 35–37.

Finally, Fig. 53 shows overall strain energy stored in the membranes for each analysis case. Differences between gravity, no gravity–NRN, and no gravity–sag shape cases did not appear, which indicates that effects of an applied gravity force on strain energy were negligible. This is because the magnitude of strain energy given by the self-weight case was three orders (1000 times) lower than for wrinkled membranes simulated as in the other three cases of Figs. 44–49. This result confirms a conclusion already stated, which is that the effects of an initial stress field caused by gravity on final deformation modes are small.

Conclusions

To clarify overall behavior of wrinkled membranes in detail, a series of spectrum analyses using the two-dimensional fast Fourier transform was carried out. This spectrum evaluation method assessed effects of a varied structural scale (scale modeling), which is related to the ratio of membrane edge length to membrane thickness and gravity field on wrinkled membranes. The conclusions obtained in this paper are summarized here:

1) The spectrum evaluation method is a good analysis tool for quantitatively assessing overall behavior of membranes with respect to both the wrinkled and slack regions.

2) When structural scale is greater than 1500, the relationship between maximum displacement (amplitude) ratio and structural scale is slightly nonlinear for each of the wrinkling analysis cases; however, this same relationship for the self-weight analysis is linear.

3) The abundance of short- and long-wavelength components simultaneously decrease and increase, respectively, as structural scale decreases, as is indicated by power-spectral-density levels. Also, membrane regions dominated by short-wavelength components are extended as structural scale decreases.

4) The most significant affects of structural scale on power spectral density appear for orientation angles in the region of 0–60 deg and are most concentrated in the regions of 30–60 deg, as structural scale increases. Power spectral densities for orientation components in the range of 0–60 deg is most dominated by short-wavelength components, which correlate to wrinkled, not slack regions.

5) Effects of the initial stress field as a result of gravity on wrinkled membranes are small, but the effects of initial deformation modes on wrinkled membranes are large. As a result, the effects of an initial stress field on final stresses in the vicinity of bifurcation points, as a result of the (1-g) gravity effect, are essentially negligible.

6) The effects of structural scale on deformation modes for all wrinkling analysis cases are most acute in wrinkled regions, whereas the gravity field effects on deformation modes are most dominant in slack regions. Based on this conclusion, it is believed that ground experiments carried out on prototype gossamer space structure hardware would accurately predict the behavior of wrinkled (but not slack) regions in space for geometry similar to that of the virtual membrane presented herein.

Acknowledgment

We thank H. Noguchi for providing support with respect to incorporating the mixed interpolation of tensorial components shell element into Finite Element Analysis Program: Personal Version.

References

[1]Johnston, J., and Lienard, S., "Modeling and Analysis of Structural Dynamics for a One-Tenth Scale Model NSGT Sunshield," AIAA Paper 2001-1407, 2001.

[2]Blandino, J. R., Johnston, J. D., Miles, J. J., and Soplop, J. S., "Thin Film Membrane Wrinkling Due to Mechanical and Thermal Loads," AIAA Paper 2001-1345, 2001.

[3]Murphey, T. W., Murphey, D. W., Mikulas, M. M., and Adler, A. L., "A Method to Quantify the Thrust Degradation Effects of Structural Wrinkles in Solar Sails," AIAA Paper 2002-1560, 2002.

[4]Johnston, J., "Finite Element Analysis of Wrinkled Membrane Structures for Sunshield Applications," AIAA Paper 2002-1456, 2002.

[5]Stein, M. S., and Hedgepeth, J. M., "Analysis of Partly Wrinkled Membrane," NASA TN D-813, July 1961.

[6]Wu, C. H., "The Wrinkled Axisymmetric Air Bags Made of Inextensible Membrane," *Journal of Applied Mechanics*, Vol. 41, No. 4, 1974, pp. 963–968.

[7]Jenkins, C. H., Haugen, F., and Spicher, W. H., "Experimental Measurement to Wrinkling in Membranes Undergoing Planer Deformation," *Experimental Mechanics*, Vol. 38, No. 2, 1998, pp. 147–152.

[8]Roddeman, D. G., Drukker, J., Oomens, C. W. J., and Janssen, J. D., "Wrinkling of Thin Membranes: Part I—Theory," *Journal of Applied Mechanics*, Vol. 54, Dec. 1987, pp. 884–887.

[9]Roddeman, D. G., Drukker, J., Oomens, C. W. J., and Janssen, J. D., "Wrinkling of Thin Membranes: Part II—Numerical Analysis," *Journal of Applied Mechanics*, Vol. 54, Dec. 1987, pp. 888–892.

[10]Kang, S., and Im, S., "Finite Element Analysis of Dynamic Response of Wrinkling Membranes," *Computer Methods in Applied Mechanics and Engineering*, Vol. 173, March 1998, pp. 227–240.

[11]Adler, A. L., Mikulas, M. M., and Hedgepeth, J. M., "Static and Dynamic Analysis of Partially Wrinkled Membrane Structures," AIAA Paper 2000-1810, 2000.

[12]Nakashino, K., and Natori, M. C., "Efficient Modification Scheme of Stress-Strain Tensor for Finite Element Analysis of Wrinkled Membranes," AIAA Paper 2003-1981, 2003.

[13]Miyamura, T., "Wrinkling of Stretched Circular Membrane Under In-Plane Torsion: Bifurcation Analysis and Experiments," *Engineering Structures*, Vol. 23, Nov. 1999, pp. 1407–1425.

[14]Wong, Y. W., and Pellegrino, S., "Computation of Wrinkle Amplitudes in Thin Membranes," AIAA Paper 2002-1369, 2002.

[15]Iwasa, T., Natori, M. C., Noguchi, H., and Higuchi, K., "Geometrically Nonlinear Analysis on Wrinkling Phenomena of a Circular Membrane," Research Report on Membrane Structures, No. 16, 2003, pp. 7–14

(in Japanese); also International Conf. on Computational Experimental Engineering Sciences, Paper 225, July 2003.

[16]Iwasa, T., Natori, M. C., and Higuchi, K., "Numerical Study on Wrinkling Properties of a Circular Membrane," *Journal of the Japan Society for Aeronautical and Space Science*, Vol. 51, No. 591, 2003, pp. 184–189 (in Japanese).

[17]Iwasa, T., Natori, M. C., and Higuchi, K., "Comparative Study on Bifurcation Theory and Tension Field Theory for Wrinkling Analysis," *Journal of Structural Engineering*, Vol. 49B, March 2003, pp. 319–326 (in Japanese).

[18]Iwasa, T., Natori, M. C., and Higuchi, K., "Evaluation of Tension Field Theory for Wrinkling Analysis with Respect to the Post-Buckling Study," *Journal of Applied Mechanics*, Vol. 74, No. 4, 2004, pp. 532–540.

[19]Jacobson, M., "Quantifying Membrane Wrinkling Behavior Due to In-Plane Shear: An Analytical Study Using Shell Elements and FFT," M.S. Thesis, Dept. of Space Studies, International Space Univ., Strasbourg, France, May 2003.

[20]Bathe, K.-J., and Dvorkin, E. N., "A Formation of General Shell Elements—The Use of Mixed Interpolation of Tensorial Components," *International Journal for Numerical Methods in Engineering*, Vol. 22, July 1986, pp. 697–722.

[21]Taylor, R. L., and Zienkiewicz, O. C., "The Finite Element Method," *Building and Construction*, Vols. 1 and 2, Butterworth–Heinemann, Oxford, 2000.

[22]Noguchi, H., and Hisada, T., "An Efficient Formulation for a Shell Element Considering Finite Rotation Increments and Its Assessment," *Transaction of the Japan Society of Mechanical Engineering*, Vol. 58, No. 550, 1992, pp. 943–950.

A. Berman
Associate Editor